HHS Public Access

Author manuscript

Adv Healthc Mater. Author manuscript; available in PMC 2022 July 01.

Published in final edited form as:

Adv Healthc Mater. 2021 July ; 10(13): e2001368. doi:10.1002/adhm.202001368.

Sonosensitizer-functionalized graphene nanoribbons for adhesion blocking and sonodynamic ablation of ovarian cancer spheroids

Hak Rae Lee,
Department of Chemical Engineering and Materials Science, University of Minnesota, Minneapolis, MN 55455, USA

Dae Woo Kim,
Department of Chemical and Biomolecular Engineering, Yonsei University, Seoul 03722, Republic of Korea

Victoria Jones,
Department of Chemical Engineering and Materials Science, University of Minnesota, Minneapolis, MN 55455, USA

Yunkyu Choi,
Department of Chemical and Biomolecular Engineering, Yonsei University, Seoul 03722, Republic of Korea

Vivian E. Ferry,
Department of Chemical Engineering and Materials Science, University of Minnesota, Minneapolis, MN 55455, USA

Melissa A. Geller,
Department of Obstetrics, Gynecology and Women's Health, Division of Gynecologic Oncology, University of Minnesota, Minneapolis, MN 55455, USA

Samira M. Azarin
Department of Chemical Engineering and Materials Science, University of Minnesota, Minneapolis, MN 55455, USA

Abstract

Advanced stage ovarian cancer is challenging to treat due to widespread seeding of tumor spheroids throughout the mesothelial lining of the peritoneal cavity. In this work, a therapeutic strategy using graphene nanoribbons (GNR) functionalized with 4-arm polyethylene glycol (PEG) and chlorin e6 (Ce6), a sonosensitizer, to target metastatic ovarian cancer spheroids is reported. GNR-PEG-Ce6 adsorbs onto the spheroids and disrupts their adhesion to extracellular matrix proteins or LP-9 mesothelial cells. Furthermore, for spheroids that do adhere, GNR-PEG-Ce6 delays spheroid disaggregation and spreading as well as mesothelial clearance, key metastatic

azarin@umn.edu .

Supporting Information

Supporting Information is available from the Wiley Online Library or from the author.

processes following adhesion. Owing to the sonodynamic effects of Ce6 and its localized delivery via the biomaterial, GNR-PEG-Ce6 can kill ovarian cancer spheroids adhered to LP-9 cell monolayers when combined with mild ultrasound irradiation. The interaction with GNR-PEG-Ce6 also loosens cell-cell adhesions within the spheroids, rendering them more susceptible to treatment with the chemotherapeutic agents cisplatin and paclitaxel, which typically have difficulty penetrating ovarian cancer spheroids. Thus, this material could facilitate effective chemotherapeutic and sonodynamic combination therapies. Finally, the adhesion inhibiting and sonodynamic effects of GNR-PEG-Ce6 are also validated with tumor spheroids derived from the ascites fluid of ovarian cancer patients, providing evidence of the translational potential of this biomaterial approach.

Graphical Abstract

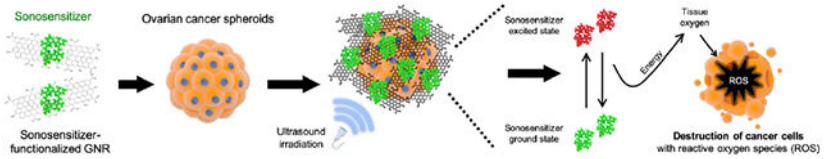

GNR functionalized with 4-arm PEG and the sonosensitizer Ce6 associates with ovarian cancer spheroids and forms a physical barrier that disrupts mesothelial adhesion of the spheroids. Combined with ultrasound irradiation, GNR-PEG-Ce6 kills ovarian cancer spheroids adhered to LP-9 mesothelial cell monolayers via sonodynamic effects, suggesting that this approach can reduce ovarian cancer metastasis in the peritoneal cavity.

Keywords

graphene nanoribbons; graphene oxide; ovarian cancer; sonodynamic therapy; ultrasound irradiation

1. Introduction

Development of therapeutic strategies that reduce metastatic spread of cancer spheroids in the peritoneal cavity has been a key challenge in ovarian cancer treatment. Ovarian cancer spheroids disseminating from the primary tumor are transported throughout the peritoneal cavity by ascites fluid and eventually adhere to the peritoneal organs covered by a mesothelial cell layer.[1-3] This unique mode of ovarian cancer metastasis allows for widespread metastases to develop simultaneously within the peritoneal cavity, making surgical removal challenging. One therapeutic approach has been to disrupt integrin-mediated interactions with extracellular matrix (ECM) proteins on the mesothelial layer that mediate mesothelial adhesion of ovarian cancer spheroids.[4] For example, a monoclonal antibody against integrin β1 subunits significantly blocked mesothelial adhesion of ovarian cancer spheroids *in vitro* and *in vivo*.[4-6] Despite their potential in preclinical studies, none of the integrin blocking approaches have demonstrated clinical benefit thus far, indicating that inhibition of a single type of integrin is not sufficient to prevent metastatic spread of ovarian cancer or that non-integrin associated pathways are also involved.[1,4,6-8] Thus, a

novel therapeutic strategy to reduce the seeding of ovarian cancer spheroids throughout the peritoneal cavity is needed.

Graphene-based materials including graphene oxide (GO) and graphene nanoribbons (GNR) have shown potential in biomedical applications including cancer therapy due to their unique physical and chemical properties.[9-11] For example, the presence of various functional groups (e.g. hydroxyl, epoxyl, and carboxyl groups) in their chemical structure allows for additional functionalization to ensure high solubility and stability in physiological solutions and to facilitate drug and biomolecule loading.[12,13] Furthermore, the presence of these functional groups and a polyaromatic domain enable graphene-based materials to adsorb ECM proteins through hydrophobic interactions, electrostatic forces, and hydrogen bonding, enabling cell adhesion to graphene-based materials.[14] Previous studies found that adhesion of mesenchymal stem cells to graphene-based materials involves surface adhesion receptors also implicated in mesothelial adhesion of ovarian cancer spheroids, such as integrin β1, suggesting that graphene-based materials may be able to target integrin receptors on the ovarian cancer spheroids.[15,16]

The hydrophobic polyaromatic domain of graphene-based materials can also provide exceptionally high loading capacity of aromatic drug molecules via pi-pi stacking, making these materials a versatile carrier for a wide variety of chemotherapeutic drugs.[12,17-19] Recently, graphene-based materials have also been integrated with sensitizing agents that generate cytotoxic effects upon external triggers such as light or ultrasound for tumor-specific treatment.[11,20] Graphene-based materials have widely been employed as a carrier for photosensitizers in photodynamic therapy, but the low penetration depth of light limits the efficacy of photodynamic therapy for deep-seated tumors.[11,21,22] As compared to conventional photodynamic therapy, sonodynamic therapy using ultrasound and a sonosensitizer has shown better therapeutic potential, with high tissue-penetrating ability when combined with graphene-based materials.[20,23] Thus, we hypothesized that targeting metastatic ovarian cancer spheroids with sonosensitizer-loaded graphene-based materials could block the mesothelial adhesion of the spheroids as well as kill the spheroids via targeted delivery of sonosensitizers coupled with ultrasound irradiation.

In this work, two graphene-based materials, GO, a single or few-layered two-dimensional carbon sheet, and GNR, narrow strips of unzipped multi-walled carbon nanotubes (MWNTs), were tested to target ovarian cancer spheroids. Our results demonstrated that GNR functionalized with 4-arm polyethylene glycol (GNR-PEG) exhibited enhanced cytocompatibility toward healthy mesothelial cells and better tumor spheroid adhesion blocking effects than GO-PEG. Importantly, GNR-PEG provided more sustained adhesion blocking effects compared to conventional antibody blocking approaches. In addition, GNR-PEG loaded with sonosensitizer Ce6 (GNR-PEG-Ce6) was able to kill ovarian cancer spheroids via sonodynamic therapy. Adhesion blocking and sonodynamic effects of GNR-PEG-Ce6 were also validated with ovarian cancer spheroids derived from patient ascites fluid, providing further evidence of the therapeutic potential of this material. This approach for blocking adhesion of ovarian cancer spheroids or ablating them even once they have adhered offers a promising therapeutic strategy to reduce metastatic spread of ovarian cancer in the peritoneal cavity.

2. Results and Discussion

2.1. PEGylation of GO and GNR to reduce aggregation in the serum-rich ascites microenvironment.

GO and GNR were prepared as previously described.[24,25] X-ray photoelectron spectroscopy (XPS) results displayed characteristic peaks in the synthesized GO and GNR (Figure S1). In addition, Raman spectra and transmission electron microscopy (TEM) images revealed that GNR was successfully prepared via unzipping of MWNTs (Figure S1). Since graphene-based materials are known to have low stability and exhibit significant aggregation in physiological solutions, in part due to nonspecific binding of proteins, amine-terminated 4-arm PEG was conjugated to GO and GNR via amide formation to reduce aggregation in ascites, a protein-rich body fluid.[12] FTIR spectra revealed that the signature peaks of 4-arm PEG, a C-O stretch (red region at ~1100 cm^{-1}, Figure 1A) and a COO-H/O-H stretch (blue region at ~2850 cm^{-1}), appeared on GO-PEG and GNR-PEG. In addition, as a consequence of amide formation, a C=O stretch (yellow region at ~1640 cm^{-1}) appeared in GO-PEG and GNR-PEG.[12] The addition of PEG to GO and GNR was also evidenced by the increase in zeta potential due to the amide formation between amine groups in 4-arm PEG and carboxyl groups in GO and GNR (Figure S2). Scanning electron microscope (SEM) images revealed no significant morphological changes in GO and GNR after PEGylation (Figure 1B). To evaluate aggregation after PEGylation, 100 μg mL^{-1} of GO, GNR, GO-PEG or GNR-PEG were suspended in cell culture media containing 20% (v/v) serum, to mimic protein-rich ascites fluid, and monitored over time after brief sonication. The delayed aggregation of GO-PEG and GNR-PEG compared to bare GO and GNR in serum-supplemented cell culture media is indicative of reduced aggregation following the addition of PEG, with no significant aggregation observed in GNR-PEG at 48 h (Figure 1C). PEGylation also reduced aggregation in phosphate-buffered saline (PBS) (Figure S3). Next, GO-PEG and GNR-PEG were tested with LP-9 human mesothelial cells, a major cellular component in the peritoneal cavity, to evaluate their biocompatibility. While GNR-PEG did not induce any decrease in viability or proliferation of the LP-9 cell layer, GO-PEG significantly reduced the viability, integrity, and proliferation of the mesothelial cell layer at concentrations higher than 50 μg mL^{-1} (Figure S4), suggesting that GNR-PEG is more cytocompatible than GO-PEG.

2.2. GO-PEG and GNR-PEG adsorb to ovarian cancer spheroids and disrupt their adhesion to ECM proteins abundant in the mesothelial layer.

The SKOV-3 cell line was used to evaluate the interactions between GO-PEG or GNR-PEG and ovarian cancer cells, since this cell line was derived from the ascites fluid of an ovarian cancer patient.[26] Cancer spheroids were generated using an established method (Figure S5A); SKOV-3 cells placed in culture on a non-adhesive poly(2-hydroxyethyl methacrylate) (pHEMA) surface spontaneously aggregated and formed spheroids (Figure S5B).[27-29] After 24 h, the spheroids ranged from 55 to 330 μm in size (Figure S5B), which is in the clinically observed size range of cancer spheroids in patient ascites (30-200 μm).[4,5] Thus, the spheroid formation step was performed for 24 h for all remaining studies. After formation, spheroids were incubated with GO-PEG or GNR-PEG at various concentrations (50-100 μg mL^{-1}) for 48 h. Optical microscope and SEM images revealed that GO-PEG and

GNR-PEG adsorbed onto SKOV-3 spheroids, forming a barrier layer covering the surface of the spheroids (Figure 2A). One-dimensional strands of GNR-PEG appeared to be entangled on the surface, forming a dense layer, while two-dimensional GO-PEG formed a thin layer along the surface of the spheroids (Figure S6).

The ability of these barrier layers of GO-PEG and GNR-PEG to disrupt integrin-mediated adhesion was evaluated using collagen I, IV, and fibronectin, the most abundant ECM proteins in the mesothelial layer.[1] When GO-PEG- or GNR-PEG-treated SKOV-3 spheroids were transferred to ECM protein-coated surfaces in serum-free media, the spheroids displayed significantly inhibited adhesion to collagen I, IV, and fibronectin over 3 days, whereas all untreated SKOV-3 spheroids adhered (Figure 2B). These results suggest that the physical barrier of GO-PEG/GNR-PEG on the surface could interfere with surface receptor-ECM protein interactions. In comparison, a conventional approach using antibody blocking of surface receptors such as integrin β1 or CD44, which have been shown to inhibit spheroid adhesion to ECM proteins for short time periods (2 h) in previous studies, did not have considerable blocking effects over 3 days under these conditions (Figure S7).[4,5] Increasing the concentration of GO-PEG or GNR-PEG from 50 to 100 μg mL^{-1} led to a decrease in adhesion rate, suggesting that higher concentrations provide better blocking effects. Since GNR-PEG exhibited greater adhesion blocking effects and cytocompatibility than GO-PEG, GNR-PEG was used for the remaining studies.

Following adhesion, metastasizing ovarian cancer spheroids disaggregate and spread rapidly, with tumor areas growing in size up to 200-fold in a week, in order to establish secondary tumors in the mesothelial lining.[30] While untreated adhered SKOV-3 spheroids exhibited an average spreading distance of 58 ± 15 μm at 4 h, adhered GNR-PEG-treated spheroids did not exhibit any visible spreading at this timepoint (Figure S8). Furthermore, the average spreading distance of untreated spheroids over 24 h was significantly higher compared to that of GNR-PEG-treated SKOV-3 spheroids, indicating that the barrier layer of GNR-PEG inhibits disaggregation and spreading of adhered spheroids (Figure S8). It was previously found that disaggregation and spreading of ovarian cancer spheroids are also mediated by interactions between surface receptors and ECM proteins, primarily integrin β1 and collagen I.[30] Thus, the barrier layer of GNR-PEG that interferes with surface receptor-ECM protein interactions in the process of spheroid adhesion likely also inhibits disaggregation and spreading of spheroids once they have adhered.

2.3. Chlorin e6 (Ce6) loaded onto GNR-PEG enhances adhesion blocking effects of GNR-PEG by downregulating surface receptor proteins.

Although coating the surface of ovarian cancer spheroids with GNR-PEG significantly inhibited their adhesion to ECM proteins, some spheroids treated with GNR-PEG were still able to adhere (Figure 2B). Thus, we sought to develop a strategy by which the adsorption of GNR-PEG onto tumor spheroids attached to the mesothelial layer could be used to kill the cancer cells. To this end, we loaded Ce6 onto GNR-PEG via pi-pi stacking, noncovalent bonding between aromatic rings. Ce6 is a naturally occurring sonosensitizer, and its anti-tumor activity in sonodynamic therapy has been confirmed with various tumors including leukemia, breast, and liver cancers.[31-33] In addition, Ce6 has been found to have selective

accumulation in the tumor and rapid clearance from normal tissues in many previous studies, which reduces the risk of side effects in normal tissues in the peritoneal cavity.[34,35] The loading of Ce6 was confirmed by UV-VIS spectrometry, in which characteristic absorption peaks of Ce6 at 400 nm and 660 nm appeared on the UV-VIS spectra of GNR-PEG-Ce6 (Figure 3A). Since a significant amount of undissolved Ce6 was visible at concentrations higher than 0.1 mg mL^{-1} due to the low solubility of Ce6 in water, 0.1 mg mL^{-1} was chosen as the concentration for Ce6 loading in our study to minimize wasted Ce6. Loading efficiency at 0.1 mg mL^{-1} was approximately 2.1% (Table S6). No significant morphological changes were found in GNR-PEG-Ce6 compared to GNR-PEG (Figure S9).

Interestingly, GNR-PEG-Ce6 exhibited greater adhesion blocking effects compared with GNR-PEG. In the *in vitro* adhesion assays, none of the SKOV-3 spheroids treated with 50 μg/mL of GNR-PEG-Ce6 were able to adhere to any of the ECM proteins by 72 h. Ce6 alone had no significant blocking effects at 50 μg mL^{-1} but it significantly disrupted spheroid adhesion to ECM proteins at 100 μg mL^{-1} (Figure 3B and S10). In addition, Ce6 led to significant changes in spheroid morphology. SKOV-3 spheroids treated with Ce6 or GNR-PEG-Ce6 displayed a grape-like morphology with loosened cell-cell adhesions compared with the tight cell-cell adhesion in the spheroids without Ce6 exposure (Figure 3C). It was found that SKOV-3 spheroids treated with 100 μg mL^{-1} of Ce6 for 48 h displayed significantly downregulated expression of E-cadherin, which mediates cell-cell adhesion. Furthermore, integrin β1 and CD44, which mediate spheroid adhesion to ECM proteins, also exhibited a significant decrease in Ce6-treated spheroids compared with untreated spheroids (Figure 3D). Ce6 loaded onto GNR-PEG was also able to significantly reduce expression of these surface receptors in SKOV-3 spheroids, whereas GNR-PEG alone did not significantly decrease their expression. It was previously reported that Ce6 inhibited integrin activation and fibrinogen binding to integrin receptors, suggesting that Ce6 could deactivate surface adhesion receptors such as integrins.[36] Thus, the enhanced adhesion blocking effects of GNR-PEG-Ce6 are likely attributed to the downregulation of surface receptors that mediate spheroid adhesion. Though Ce6 alone has adhesion blocking effects at 100 μg mL^{-1}, significant cytotoxic effects on LP-9 mesothelial cells at this dose (Figure S11A) limit its therapeutic use. In contrast, GNR-PEG-Ce6 exhibited significantly less toxicity at its effective concentrations (50-100 μg mL^{-1}, Figure S11B) where no spheroid adhesion to ECM proteins was observed, as localized delivery of Ce6 to spheroids via GNR-PEG-Ce6 allows for a lower quantity of Ce6 to achieve similar effects, significantly reducing toxicity to mesothelial cells.

2.4. GNR-PEG-Ce6 inhibits spheroid adhesion to mesothelial layer and subsequent mesothelial clearance.

While adhesion inhibiting effects of GNR-PEG-Ce6 were observed on individual ECM proteins, spheroid adhesion to ECM proteins does not fully represent the mesothelial adhesion process. It was previously found that spheroid adhesion was significantly higher on live mesothelial cells than on fixed mesothelial cells with preserved ECM proteins, suggesting the importance of live interactions between ovarian cancer spheroids and mesothelial cells in mediating spheroid adhesion.[4] Thus, to examine whether GNR-PEG-Ce6 could also disrupt mesothelial adhesion of ovarian cancer spheroids, GNR-PEG-Ce6

was tested in an ascites-like *in vitro* microenvironment in which SKOV-3 spheroids were suspended on top of a confluent LP-9 mesothelial cell layer. Then, 50 μg mL^{-1} of GNR-PEG-E6 was added to the SKOV-3 spheroid suspension with orbital shaking at 50 rpm to mimic the movement of ascites in the peritoneal cavity, a crucial factor in the peritoneal microenvironment affecting the efficacy of therapeutic intervention.[37-39]

It was found that GNR-PEG and GNR-PEG-Ce6 preferentially adsorbed onto SKOV-3 spheroids as opposed to the LP-9 cells (Figure 4A). Preferential accumulation of GNR-PEG and GNR-PEG-Ce6 on the spheroids instead of the LP-9 layer was likely attributed to the enhanced stability of the materials in serum-rich physiological buffers, which provided GNR-PEG and GNR-PEG-Ce6 more time to interact with ovarian cancer spheroids before these materials settled due to aggregation (Figure 4A). While 33 ± 8.2% of untreated SKOV-3 spheroids adhered to the LP-9 cell layer at 4 h, GNR-PEG- or GNR-PEG-Ce6-treated SKOV-3 spheroids were not able to adhere by that timepoint (Figure 4B). Furthermore, over 90% of untreated SKOV-3 spheroids and 40% of GNR-PEG-treated spheroids adhered to LP-9 cell layer by 72 h, whereas less than 2% of SKOV-3 spheroids treated with GNR-PEG-Ce6 were able to adhere in 72 h. This is likely attributed to the synergistic effects from the reduced expression of surface receptors by Ce6 and the barrier layer of GNR-PEG-Ce6. In comparison to GNR-PEG-Ce6, the conventional approach of blocking integrin β1 or CD44 with antibodies did not effectively inhibit mesothelial adhesion under the same experimental conditions. More than 80% of spheroids were able to adhere to LP-9 monolayer by 24 h in all groups regardless of blocking (Figure S12), indicating that directly blocking surface receptors does not provide the longer-term efficacy of GNR-PEG-Ce6.

GNR-PEG-Ce6 also inhibited subsequent spreading of adhered spheroids on the mesothelial layer. Following adhesion on the mesothelial layer, metastasizing spheroids spread by clearing mesothelial cells from their path at adhesion sites, a phenomenon termed mesothelial cell clearance, in a talin-1- and integrin α5β1-dependent manner.[40,41] This has also been observed in clinical biopsies of patient tumors attached to peritoneal organs showing the absence of mesothelial cells underneath the attached tumor.[40] In our study, LP-9 cells underneath untreated SKOV3 spheroids exhibited clearance in 2 h (Figure 4C), which is consistent with the previous finding that tumor spheroids began clearing the mesothelial layer 30 min after spheroid attachment.[42] In contrast, LP-9 cells beneath the SKOV-3 spheroids treated with GNR-PEG or GNR-PEG-Ce6 displayed significantly delayed clearance, with the lowest level of clearance observed with GNR-PEG-Ce6. After 24 h of incubation, clearance of the LP-9 cell layer was visible in all groups except GNR-PEG-Ce6, which displayed no sign of clearance over a 24 h period. The delay observed in mesothelial clearance could be in part due to the downregulation of integrin α5β1, a key player in mesothelial clearance, as western blot analysis revealed that GNR-PEG-Ce6 downregulates integrin α5 as well as β1 (Figure 3D and Figure S13), and blocking α5β1 integrin was found to decrease mesothelial clearance in a previous study.[40]

GNR-PEG-Ce6 can kill ovarian cancer spheroids via sonodynamic therapy and enhance the efficacy of adjuvant chemotherapy.

To evaluate whether sonodynamic therapy using GNR-PEG-Ce6 could kill adhered ovarian cancer spheroids, SKOV-3 spheroids placed on top of a confluent LP-9 cell monolayer were treated with 50 μg mL^{-1} of GNR-PEG-Ce6 for 48 h, with orbital shaking at 50 rpm. Non-adhered spheroids were removed after 48 h of treatment, and ultrasound irradiation was delivered from the top (Figure 5A). No significant cell death was observed prior to ultrasound irradiation in all conditions: untreated, GNR-PEG-treated, and GNR-PEG-Ce6-treated (Figure 5B). After 30 s of 0.8 W cm^{-2} ultrasound irradiation at a frequency of 1 MHz, massive cell death was detected in GNR-PEG-Ce6-treated spheroids adhered to the LP-9 layer (Figure 5B). Furthermore, GNR-PEG-Ce6-treated spheroids detached from the LP-9 layer during the ultrasound irradiation, suggesting weak adhesion between the spheroids and LP-9 layer. In addition to the spheroids adhered to the LP-9 layer, GNR-PEG-Ce6-treated spheroids that had not adhered to the LP-9 cells were also completely killed when ablated separately with the same level of ultrasound irradiation (Figure S14), indicating that these materials could potentially be used to apply sonodynamic therapy to both tumor cells adhered to the mesothelial lining and those suspended in the ascites fluid in patients. Ultrasound irradiation alone triggered no significant cell death in SKOV-3 spheroids or LP-9 monolayers. Some cell death was also observed in GNR-PEG-treated spheroids after ultrasound irradiation, but it was not as significant as in the GNR-PEG-Ce6-treated spheroids, suggesting that the sonosensitizing effect of Ce6 contributed to cell death in GNR-PEG-Ce6-treated spheroids (Figure 5B). Cell death by sonodynamic therapy has been shown to be mediated by the generation of reactive oxygen species (ROS), which trigger apoptotic pathways within cells.[35] It was found that ROS generation upon ultrasound irradiation was significantly higher in GNR-PEG-Ce6-treated SKOV-3 spheroids compared with other groups (Figure 5C). GNR-PEG also increased ROS generation upon ultrasound irradiation in SKOV-3 spheroids but not to the same level as GNR-PEG-Ce6 (Figure 5C). In addition, ROS generation in LP-9 cells was not significantly affected after ultrasound irradiation, likely due to the preferential accumulation of GNR-PEG-Ce6 on SKOV-3 spheroids over LP-9 cells (Figure 5D). Furthermore, GNR-PEG-Ce6 was not confined to the surface but actually penetrated deep into the SKOV-3 spheroids, allowing the delivery of Ce6-induced sonodynamic effects throughout the spheroids (Figure 5E).

GNR-PEG-Ce6 also enhanced the efficacy of chemotherapy, which could be used as an adjuvant treatment to kill residual ovarian cancer spheroids after sonodynamic therapy. Current adjuvant chemotherapy for advanced stage ovarian cancer typically uses platinum- or taxane-based drugs, but ovarian cancer spheroids have been found to have enhanced resistance to these drugs for many reasons, including poor drug penetration and the presence of a number of cell-cell junctions in spheroids.[43-48] For example, cisplatin, a platinum-based drug widely used for ovarian cancer, has shown limited penetration, being confined to the peripheral layer of cancer spheroids (0-30 μm) in previous studies.[49,50] Consistent with these previous findings, chemotherapy alone with cisplatin or paclitaxel was not able to induce significant cell death in SKOV-3 spheroids (Figure S15). However, significant death was observed in GNR-PEG-Ce6-treated spheroids at the same chemotherapy dose (Figure S15). This is likely due to the fact that the loosened cell-cell junctions in GNR-

PEG-Ce6-treated spheroids enhanced the penetration of cisplatin or paclitaxel, whereas a barrier of tight cell-cell junctions in untreated and GNR-PEG-treated spheroids did not allow those drugs to penetrate throughout. Indeed, it was previously reported that epithelial junction opener (JO-1) improved the efficacy of co-administered chemotherapeutic drugs by loosening cell-cell junctions in an ovarian cancer model.[47,48] These results suggest that GNR-PEG-Ce6 can be combined with conventional chemotherapy to kill ovarian cancer spheroids in the peritoneal cavity, offering an additional therapeutic route with this material.

GNR-PEG-Ce6 can disrupt mesothelial adhesion of ovarian cancer spheroids in patient ascites and kill them via sonodynamic therapy.

Lastly, to demonstrate the translational potential of this material, GNR-PEG-Ce6 was tested with patient ascites spheroids. Prior to the studies, staining of the spheroids with ovarian cancer marker cancer antigen 125 (CA125) and cytokeratin 7 (CK7) verified that they contained tumor cells (Figure 6A). GNR-PEG-Ce6 was able to adsorb onto patient ascites spheroids by 48 h of treatment (Figure 6B and Figure S16), forming a barrier layer on the outer surface. To evaluate adhesion, patient ascites spheroids were mixed with 50 μg mL^{-1} GNR-PEG-Ce6 and placed above a confluent LP-9 cell layer. While the adhesion rate of untreated ascites spheroids after 72 h of incubation was lower compared to that of SKOV-3 spheroids, GNR-PEG-Ce6 significantly inhibited adhesion of patient ascites spheroids in all patient samples (Figure 6C). When 30 s of 0.8 W cm^{-2} ultrasound irradiation was applied to GNR-PEG-Ce6-treated spheroids, ROS generation significantly increased (Figure 6D), and significant cell death was also observed in patient ascites spheroids adhered to LP-9 layers (Figure 6E). GNR-PEG-Ce6-treated patient ascites spheroids that had not adhered to LP-9 layers could be also be destroyed by ultrasound irradiation (Figure S17). These results collectively demonstrate that GNR-PEG-Ce6 combined with sonodynamic therapy has therapeutic potential for advanced stage ovarian cancer patients.

3. Conclusion

There is an urgent need for development of alternative treatment options for ovarian cancer, which is typically diagnosed at advanced stages in which tumor spheroids have spread throughout the abdominal cavity. In this study, we report a novel material-based therapeutic strategy using GNR functionalized with 4-arm PEG and the sonosensitizer Ce6 to reduce metastatic spread of ovarian cancer within the peritoneal space. Our results demonstrate that GNR-PEG-Ce6 can adsorb to the surface of ovarian cancer spheroids, forming a physical barrier layer which disrupts mesothelial adhesion of the spheroids. GNR-PEG-Ce6 also significantly delays disaggregation and spreading as well as mesothelial clearance of adhered spheroids, key steps in the establishment of ovarian cancer metastases. In addition, when combined with ultrasound irradiation, GNR-PEG-Ce6 kills SKOV-3 spheroids adhered to LP-9 mesothelial cell monolayers via sonodynamic effects with minimal off-target damage, suggesting that this approach can eliminate residual tumors in the peritoneal cavity. Furthermore, GNR-PEG-Ce6 can enhance the efficacy of conventional platinum- or taxane-based chemotherapy in killing the ovarian cancer spheroids, offering another therapeutic route with this material. The efficacy of GNR-PEG-Ce6 was also validated with ovarian cancer spheroids derived from patient ascites, demonstrating the translational potential of

GNR-PEG-Ce6 for future clinical use. The ability of GNR-PEG-Ce6 to target metastatic cancer spheroids in the peritoneal cavity via minimally invasive sonodynamic therapy as well as to enhance conventional chemotherapy provides promising novel strategies for targeting intraperitoneal spread of ovarian cancer.

4. Experimental Section

Synthesis of GO/GNR:

GO was synthesized via the modified Hummer's method.[24] Briefly, graphite powder (2 g; Sigma-Aldrich 282863) was dispersed in a 98% sulfuric acid solution followed by the slow addition of potassium permanganate (7 g; $KMnO_4$; Sigma-Aldrich 223468) to the mixture. The mixture was incubated at 35°C for 2 h in a water bath. Next, DI water (200 mL) was slowly added to the mixture in an ice bath. Then, hydrogen peroxide (10 mL; H_2O_2; Sigma-Aldrich H1009) was added. The resulting GO solution was filtered through a paper filter and repeatedly washed in a 10% (v/v) hydrochloric acid and deionized (DI) water solution to remove the remaining manganese impurities. The prepared GO was resuspended in DI water and lyophilized for at least 48 h. GNR was also prepared as previously described.[25] To prepare GNR, multiwalled carbon nanotubes (1 g; Hanwha Chemical CM150) were dispersed in 98% sulfuric acid (100 mL) with vigorous stirring. Then, $KMnO_4$ (3.5 g) was slowly added to the dispersion and stirred at 35 °C for 15 h. Deionized water (100 mL) was slowly added to this solution in an ice bath. Next, H_2O_2 (100 mL) was slowly added to the mixture to terminate the oxidation of carbon nanotubes by $KMnO_4$. To remove the acidic reaction solution, GNR was centrifuged at 15,000 rpm for 1 hour at 4°C, and precipitated GNR was washed in DI water several times. The purified GNR was resuspended in DI water and lyophilized for at least 48 h. XPS was conducted using a K-alpha XPS system (Thermo Fisher Scientific). TEM imaging of synthesized GO and GNR was performed using a field emission transmission electron microscope (JEM-F200, JEOL). Raman spectra of GNR and MWNT were obtained using a laser of 532 nm wavelength (LabRam Aramis, HORIBA Jobin Yvon). Zeta potentials were measured at pH 7.0 by diluting 10 μL of the material solution (2 mg mL^{-1}) in 10 mL DI water (ELSZ-2000ZS, Otsuka Electronics).

PEGylation of GO or GNR:

For PEGylation with 4-arm PEG, GO or GNR were diluted to 1 mg mL^{-1}. Amine-terminated 4-arm PEG (5 mg mL^{-1}; average Mn = 2,000; Sigma-Aldrich JKA7032) was added to the GO or GNR solution and bath-sonicated for 5 min. Then, 1-ethyl-3-(3-dimethylaminopropyl)carbodiimide hydrochloride (5 μM; EDC; Thermo Fisher Scientific 22980) was added to the mixture and bath-sonicated for 30 min. Additional EDC was added to mixture to the final concentration of 20 μM, and the mixture was stirred overnight at room temperature. To remove unbound 4-arm PEG, the resulting GO-PEG or GNR-PEG solution was centrifuged at 15,000 rpm for 1 hour, and precipitated GO-PEG or GNR-PEG were resuspended in sterile water at a final concentration of 1 mg mL^{-1}. PEGylation was confirmed with Fourier-transform infrared spectroscopy (FTIR) using the Nicolet 6700 FTIR spectrometer (Thermo Fisher Scientific). To evaluate stability in physiological buffers, GO-PEG or GNR-PEG were suspended in cell culture media containing 20% (v/v) fetal bovine serum (FBS; Thermo Fisher Scientific 16000044) and 1% (v/v) penicillin-

streptomycin (PS; Thermo Fisher Scientific 15140122). Aggregation was monitored over 24 h after a brief sonication.

Synthesis and characterization of GNR-PEG-Ce6:

Ce6 (Santa Cruz Biotechnology sc-263067) was dissolved in dimethyl sulfoxide (DMSO), followed by dilution in water to achieve the desired final concentration. For Ce6 loading onto GNR-PEG, Ce6 was added to GNR-PEG (1 mg mL^{-1}) in water to the final concentration of 0.01 mg mL^{-1} and stirred overnight at room temperature. Unloaded excess Ce6 in the supernatant was removed after brief centrifugation of GNR-PEG-Ce6 followed by washing in water. This step was repeated until the green color of Ce6 in the supernatant disappeared. UV-Vis spectrometry was performed using the Evolution 220 UV-Visible spectrophotometer (Thermo Fisher Scientific) to evaluate Ce6 loading. The signature peak of Ce6 at 400nm in UV-Vis spectra was used to determine loading efficiency with a molar extinction coefficient of 1.5×10^5 M^{-1} cm^{-1} at 400 nm[51] and the Beer-Lambert equation described below.

$$A = \varepsilon LC \quad (1)$$

A, ε, L, and C in equation (1) indicate the amount of light absorbed by the sample for a particular wavelength, the molar extinction coefficient, the distance that the light travels through the solution, and the concentration of the absorbing species per unit volume, respectively.

Cell culture:

SKOV-3 human ovarian cancer cells (ATCC HTB-77) were maintained in McCoy's 5A media (Thermo Fisher Scientific 16600) supplemented with 10% (v/v) FBS and 1% (v/v) PS. LP-9 human peritoneal mesothelial cells (Coriell Institute AG07085) were maintained in flasks pre-coated with gelatin (0.1 w/v%; STEMCELL Technologies 07903) in media prepared by mixing Dulbecco's Modified Eagle Media (DMEM, Sigma-Aldrich D6429) and Media 199 (GE Healthcare Life Science SH30253.01) in a 1:1 ratio, supplemented with 15% FBS, epidermal growth factor (10 ng mL^{-1}; EGF; PeproTech AF-100-15), and hydrocortisone (0.4 μg mL^{-1}; Sigma-Aldrich H0888-1G).

Cancer spheroid generation on pHEMA-coated plates:

To make the poly(2-hydroxyethyl methacrylate) (pHEMA, Sigma-Aldrich P3932) solution, pHEMA pellets (1.2 g) were dissolved in 95% ethanol in water (38 mL). The solution was stirred overnight at room temperature, then sterile-filtered using a tube top filter unit (MilliporeSigma SCGP00525) and stored at 4 °C prior to future use. Cell culture plates were coated with pHEMA (15 μL cm^{-2}) and dried overnight at room temperature in a biosafety cabinet. For spheroid generation, SKOV-3 cells (2 million) suspended in maintenance media (10 mL) were plated on a 100 mm diameter pHEMA-coated culture dish. Spheroid size, represented as an average of two perpendicular diameters, was measured using ImageJ software.

Purification of patient ascites spheroids:

Ascites fluid samples from patients newly diagnosed with stage III or IV serous ovarian carcinoma were kindly provided by Dr. Amy P.N. Skubitz and were obtained through the University of Minnesota Cancer Center Tissue Procurement Facility with approval of the University of Minnesota Institutional Review Board (Protocol 0702E01841). Written informed consent was received from all participants prior to collection of the ascites samples. Tumor spheroids were isolated from the ascites fluid as previously described.[52] Patient ascites spheroids were maintained on a pHEMA-coated culture dish in McCoy's 5A media supplemented with 10% (v/v) FBS and 1% (v/v) PS.

Treatment with graphene-based materials or monoclonal antibodies (mAbs):

SKOV-3 spheroids were cultured on a pHEMA-coated dish in McCoy's 5A media supplemented with 10% (v/v) FBS and 1% (v/v) PS for 24h before treatment with graphene-based materials or mAbs. Graphene-based materials or mAbs were directly added to the media and incubated with SKOV-3 spheroids for 48 h. The mAbs (100 μg mL^{-1}) used for blocking surface receptors are listed in Table S1.

Spheroid adhesion tests on ECM proteins:

For adhesion tests, 96-well plates with non-tissue culture treated surfaces were coated with collagen I (50 μg mL^{-1}; Corning 354249), collagen IV (50 μg mL^{-1}; Sigma-Aldrich C5533), or fibronectin (50 μg mL^{-1}; Sigma-Aldrich F1141) in distilled water and incubated overnight at 37 °C prior to spheroid plating. Spheroids were resuspended in serum-free McCoy's 5A media, and the suspension (100 μL) was added to each well of a 96-well plate, resulting in 50-100 spheroids per well. The total number of spheroids in each well was manually counted prior to incubation. After incubation, non-adhered spheroids were washed out and the number of remaining spheroids was counted. The percentage of adhered spheroids in each well was calculated as the number of remaining spheroids divided by the total number of spheroids before incubation.

Spheroid adhesion test on LP-9 mesothelial cell layer:

LP-9 mesothelial cells were cultured on gelatin-coated 6-well plates until a confluent monolayer was formed. Then, SKOV-3 spheroids cultured for 24 h on the pHEMA-coated surface were mixed with GNR-PEG (50 μg mL^{-1}) or GNR-PEG-Ce6 (50 μg mL^{-1}) in the LP-9 cell maintenance media (2 mL), and 50-100 spheroids were transferred on top of the LP-9 cell monolayer. The plates were gently rotated on an orbital shaker at 50 rpm during the test. The adhesion rate was evaluated as described above for the adhesion tests on ECM proteins.

Scanning electron microscopy (SEM):

Spheroids were prepared for SEM imaging as previously described.[53] Briefly, spheroids were fixed in 2.5% (v/v) glutaraldehyde (Sigma-Aldrich G5882) in PBS for 60 min at room temperature, followed by cross-linking in 0.5% (w/w) osmium tetroxide (OsO_4; Acros Organics AC197450010) for 30 min at room temperature. Fixed spheroids were dehydrated with a graded ethanol series from 25% to 100% anhydrous ethanol. Then, dehydrated

spheroids were resuspended in hexamethyldisilazane (HMDS, Sigma-Aldrich 440191), a chemical dehydrant, and placed on a silicon wafer for drying overnight prior to imaging. Prepared spheroids were coated with 10 nm of iridium using an EM ACE600 sputter coater (Leica). For bare or PEG-conjugated GO/GNR, diluted GO/GNR solution (10 μL, 0.05 mg mL^{-1}) was dropped onto a silicon wafer and dried in a vacuum oven at 100 °C for 2 h. The samples were coated with 2 nm of iridium using the EM ACE600 sputter coater. Imaging was performed at 2 kV accelerating voltage using a field emission gun scanning electron microscope (SU-8230, Hitachi).

Spheroid disaggregation and spreading assay:

For the spheroid disaggregation and spreading assay, 24-well plates were coated with collagen I, IV, or fibronectin (50 μg/mL) overnight at 37 °C prior to spheroid seeding. Spheroids treated with GO-PEG or GNR-PEG for 48 hours were suspended in 10% serum-supplemented McCoy's 5A media and transferred to the ECM protein-coated plates. The spheroids that had not adhered were washed out after 2 h of incubation. The adherent spheroids were imaged at 4 and 24 h after the final wash using the EVOS FL Auto fluorescence microscope (Thermo Fisher Scientific). To evaluate the average spreading distance of adhered spheroids, the four farthest distances between the outer boundary of spreading cell layer and the boundary of non-disaggregated center of adhered spheroids at each time point were measured using ImageJ software.

Histological analysis:

Spheroid fixation, embedding, sectioning, and hematoxylin and eosin staining were performed as previously described.[54]

Immunofluorescence assays:

Immunofluorescence staining was performed as previously described.[54] Primary and secondary antibodies used for staining are listed in Tables S2 and S3. Imaging was conducted with an EVOS FL Auto fluorescence microscope.

Western blot analysis:

Western blots were performed as previously described.[54] Whole cell lysate was used for detection of integrin α5, integrin β1, CD44, E-cadherin, and talin-1 (20 μg), and β-actin (10 μg). Primary and secondary antibodies used in Western blot analysis are listed in Tables S4 and S5.

Assessing cell viability:

The Live/Dead cell viability assay (Thermo Fisher Scientific L3224) and alamarBlue assay (Thermo Fisher Scientific DAL10250) were performed as previously described to evaluate the toxicity of graphene-based materials to the LP-9 cell monolayer.[54]

Evaluating mesothelial clearance:

SKOV-3 spheroids were treated with GNR-PEG or GNR-PEG-Ce6 (50 μg mL^{-1}) for 48 h before being transferred on top of a confluent LP-9 cell monolayer in 6-well plates.

The LP-9 cell layer was stained with CellTracker™ Green Dye (Thermo Fisher Scientific C2925) for 30 min prior to incubation with the spheroids. The SKOV-3 spheroids were labeled with CellTracker™ Red Dye (Thermo Fisher Scientific C34552) 1 h prior to seeding on top of LP-9 cells. The clearance of LP-9 cells underneath the spheroids was monitored and imaged using an EVOS FL Auto fluorescence microscope every hour.

Ultrasound irradiation of adhered spheroids:

SKOV-3 spheroids mixed with GNR-PEG (50 μg mL^{-1}) or GNR-PEG-Ce6 (50 μg mL^{-1}) in the LP-9 cell maintenance media (2 mL) were transferred on top of a confluent LP-9 cell monolayer in 6-well plates. The plates were gently rotated on the orbital shaker at 50 rpm for 48 h. After 48 h of treatment, non-adhered spheroids were removed, and each well was filled with media (10 mL) for ultrasound irradiation. Since SKOV-3 spheroids completely spread out in 48 h without GNR treatment, untreated spheroids adhered to the LP-9 layer at 6 h of incubation were used as the control to achieve similar levels of adhesion and disaggregation compared to the GNR-PEG-treated or GNR-PEG-Ce6-treated spheroids. Ultrasound irradiation was delivered using an ultrasound unit with 4 cm^2 transducer (LG MedSupply LG-US1). The transducer was immersed in the media and 0.8 W cm^{-2} of ultrasound irradiation at a frequency of 1Mhz was delivered for 30 s. The Live/Dead assay was performed 30 min after ultrasound irradiation.

ROS detection in SKOV-3 spheroids and LP-9 mesothelial cells:

The generation of ROS after ultrasound irradiation was evaluated using a DCFDA (2',7'–dichlorofluorescin diacetate) - Cellular ROS Assay Kit (Abcam ab113851). As in the previous adhesion test, SKOV-3 spheroids mixed with GNR-PEG-Ce6 (50 μg mL^{-1}) were placed on top of a confluent LP-9 layer in a 96-well plate rotated at 50 rpm. After 48 h of incubation, the LP-9 layer and SKOV-3 spheroids were separated and washed once with ROS staining buffer followed by staining with 20 μM of DCFDA for 30 min (LP-9 monolayer) or 60 min (SKOV-3 spheroids) at 37 °C. The stained samples were washed once with ROS staining buffer, and the fluorescence signal was measured using a Synergy H1 spectrophotometer (BioTek). Then, 0.8 W cm^{-2} of ultrasound irradiation at a frequency of 1Mhz was delivered for 30 s. After ultrasound irradiation, fluorescence signal was measured again. The percent increase of ROS generation was calculated by dividing the increase in fluorescence signal after ultrasound irradiation by the initial fluorescence signal and then multiplying by 100. Treatment with Tert-butyl hydrogen peroxide (100 μM; TBHP) for 48 h was used as positive control.

Chemotherapy in combination with GNR-PEG-Ce6:

Cisplatin (Sigma-Aldrich P4394) and paclitaxel (Sigma-Aldrich T7191) were reconstituted in DMSO to 10 % (w/v) and diluted in cell culture media. SKOV-3 spheroids were treated with GNR-PEG or GNR-PEG-Ce6 for 48 h followed by exposure to cisplatin (20 μM) or paclitaxel (20 μM) for 5 days, after which cell viability was evaluated using the Live/Dead assay. Imaging was performed using the EVOS FL Auto fluorescence microscope.

Statistical analysis:

Statistical analysis was performed with GraphPad Prism, using an unpaired Student's t test to determine P values. All data are presented as mean ± standard deviation of three biological replicates from one of three representative independent experiments. Difference between groups was considered statistically significant when the P value was less than 0.05.

Supplementary Material

Refer to Web version on PubMed Central for supplementary material.

Acknowledgements

The authors would like to thank Laura Bendzick for assistance with patient ascites spheroid sample preparation, Han Seung Lee for help with SEM training and imaging, and Kateryna Artyushkova for assistance with XPS data interpretation. Parts of this work were carried out in the Characterization Facility, University of Minnesota, which receives partial support from the National Science Foundation through the MRSEC program. Research reported in this publication was supported by the National Center for Advancing Translational Sciences of the National Institutes of Health, United States, Award Number UL1TR000114. The content is solely the responsibility of the authors and does not necessarily represent the official views of the National Institutes of Health. This work was supported by the Dr. Ralph and Marian Falk Medical Research Trust Bank of America, N.A., the NIH (U54 CA210190), the Kwanjeong Educational Foundation (H.R.L.), a Doctoral Dissertation Fellowship from the Graduate School of the University of Minnesota (H.R.L.), the Research Experiences for Undergraduates (REU) Program of the National Science Foundation under Award Number DMR-1852044, and through the University of Minnesota MRSEC under Award Number DMR-1420013.

References

[1]. Lengyel E, Am. J. Pathol 2010, 177, 1053. [PubMed: 20651229]

[2]. Tan DS, Agarwal R, Kaye SB, Lancet Oncol. 2006, 7, 925. [PubMed: 17081918]

[3]. Moffitt L, Karimnia N, Stephens A, Bilandzic M, Int. J. Mol. Sci 2019, 20, 1.

[4]. Burleson KM, Casey RC, Skubitz KM, Pambuccian SE, Oegema TR Jr., Skubitz APN, Gynecol. Oncol 2004, 93, 170. [PubMed: 15047232]

[5]. Casey RC, Burleson KM, Skubitz KM, Pambuccian SE, Oegema TR, Ruff LE, Skubitz APN, Am. J. Pathol 2001, 159, 2071. [PubMed: 11733357]

[6]. Mitra AK, Sawada K, Tiwari P, Mui K, Gwin K, Lengyel E, Oncogene 2011, 30, 1566. [PubMed: 21119598]

[7]. Sawada K, Mitra AK, Radjabi AR, Bhaskar V, Kistner EO, Tretiakova M, Jagadeeswaran S, Montag A, Becker A, Kenny HA, et al., Cancer Res. 2008, 68, 2329. [PubMed: 18381440]

[8]. Bell-Mcguinn KM, Matthews CM, Ho SN, Barve M, Gilbert L, Penson RT, Lengyel E, Palaparthy R, Gilder K, Vassos A, et al., Gynecol. Oncol 2011, 121, 273. [PubMed: 21276608]

[9]. Chowdhury SM, Surhland C, Sanchez Z, Chaudhary P, Suresh Kumar MA, Lee S, Peña LA, Waring M, Sitharaman B, Naidu M, Nanomedicine Nanotechnology, Biol. Med 2015, 11, 109.

[10]. Patel SC, Lee S, Lalwani G, Suhrland C, Chowdhury MS, Sitharaman B, Ther. Deliv 2016, 7, 101. [PubMed: 26769305]

[11]. Tian B, Wang C, Zhang S, Feng L, Liu Z, ACS Nano 2011, 5, 7000. [PubMed: 21815655]

[12]. Liu Z, Robinson JT, Sun X, Dai H, J. Am. Chem. Soc 2008, 130, 10876. [PubMed: 18661992]

[13]. Lu YJ, Lin CW, Yang HW, Lin KJ, Wey SP, Sun CL, Wei KC, Yen TC, Lin CI, Ma CCM, et al., Carbon N. Y 2014, 74, 83.

[14]. Shi X, Chang H, Chen S, Lai C, Khademhosseini A, Wu H, Adv. Funct. Mater 2012, 22, 751.

[15]. Park J, Kim B, Han J, Oh J, Park S, Ryu S, Jung S, Shin JY, Lee BS, Hong BH, et al., ACS Nano 2015, 9, 4987. [PubMed: 25919434]

[16]. Kang S, Lee J, Ryu S, Kwon Y, Kim KH, Jeong DH, Paik SR, Kim BS, Chem. Mater 2017, 29, 3461.

[17]. Mullick Chowdhury S, Zafar S, Tellez V, Sitharaman B, ACS Biomater. Sci. Eng 2016, 2, 798. [PubMed: 33440577]

[18]. Liu Z, Sun X, Nakayama-Ratchford N, Dai H, ACS Nano 2007, 1, 50. [PubMed: 19203129]

[19]. Yang X, Zhang X, Liu Z, Ma Y, Huang Y, Chen Y, J. Phys. Chem. C 2008, 112, 17554.

[20]. Dai C, Zhang S, Liu Z, Wu R, Chen Y, ACS Nano 2017, 11, 9467. [PubMed: 28829584]

[21]. Yang K, Hu L, Ma X, Ye S, Cheng L, Shi X, Li C, Li Y, Liu Z, Adv. Mater 2012, 24, 1868. [PubMed: 22378564]

[22]. Li Y, Dong H, Li Y, Shi D, Int. J. Nanomedicine 2015, 10, 2451. [PubMed: 25848263]

[23]. Chen YW, Liu TY, Chang PH, Hsu PH, Liu HL, Lin HC, Chen SY, Nanoscale 2016, 8, 12648. [PubMed: 26838477]

[24]. Dimiev AM, Tour JM, ACS Nano 2014, 8, 3060. [PubMed: 24568241]

[25]. Kosynkin DV, Higginbotham AL, Sinitskii A, Lomeda JR, Dimiev A, Price BK, Tour JM, Nature 2009, 458, 872. [PubMed: 19370030]

[26]. Fogh J, Trempe G, in Hum. Tumor Cells Vitr, 1975.

[27]. Ahmed N, Stenvers KL, Front. Oncol 2013, 3 9, 1.

[28]. White EA, Kenny HA, Lengyel E, Adv. Drug Deliv. Rev 2014, 79, 184. [PubMed: 25034878]

[29]. Lawrenson K, Grun B, Gayther SA, J. Vis. Exp 2012, 1.

[30]. Burleson KM, Hansen LK, Skubitz APN, Clin. Exp. Metastasis 2005, 21, 685.

[31]. Shi H, Liu Q, Qin X, Pan W, Wang X, Biopharm. Drug Dispos 2011, 32, 319. [PubMed: 21815170]

[32]. Li Y, Wang P, Wang X, Su X, Liu Q, Ultrasound Med. Biol 2014, 40, 990. [PubMed: 24462156]

[33]. Li Q, Wang X, Wang P, Zhang K, Wang H, Feng X, Liu Q, Cancer Biother. Radiopharm 2014, 29, 42. [PubMed: 24206161]

[34]. Wang H, Wang X, Wang P, Zhang K, Yang S, Liu Q, Ultrasound Med. Biol 2013, 39, 1713. [PubMed: 23830103]

[35]. Wan GY, Liu Y, Chen BW, Liu YY, Wang YS, Zhang N, Cancer Biol. Med 2016, 13, 325. [PubMed: 27807500]

[36]. Park JY, Ji HD, Jeon BR, Im EJ, Son YM, Lee JY, Lee DH, Lee YC, Hyun E, Jia Q, et al., Evidence-based Complement. Altern. Med 2013, 2013.

[37]. Masiello T, Dhall A, Hemachandra L, Tokranova N, Melendez J, Castracane J, Cells 2018, 7, 277.

[38]. Rizvi I, Gurkan UA, Tasoglu S, Alagic N, Celli JP, Mensah LB, Mai Z, Demirci U, Hasan T, Proc. Natl. Acad. Sci. U. S. A 2013, 110.

[39]. Avraham-Chakim L, Elad D, Zaretsky U, Kloog Y, Jaffa A, Grisaru D, PLoS One 2013, 8, 0.

[40]. Kenny HA, Nieman KM, Mitra AK, Lengyel E, Cancer Discov. 2011, 1, 100. [PubMed: 22013555]

[41]. Iwanicki MP, Davidowitz RA, Ng MR, Besser A, Muranen T, Merritt M, Danuser G, Ince T, Brugge JS, Cancer Discov. 2011, 1, 144. [PubMed: 22303516]

[42]. Iwanicki MP, Davidowitz RA, Ng MR, Besser A, Muranen T, Merritt M, Danuser G, Ince T, Brugge JS, Cancer Discov. 2011, 1, 144. [PubMed: 22303516]

[43]. Mcguire Iii W, Markman M, Br. J. Cancer 2003, 89, 3.

[44]. Shield K, Ackland ML, Ahmed N, Rice GE, Gynecol. Oncol 2009, 113, 143. [PubMed: 19135710]

[45]. Mehta G, Hsiao AY, Ingram M, Luker GD, Takayama S, Control J. Release 2012, 164, 192.

[46]. Green SK, Francia G, Isidoro C, Kerbel RS, Mol. Cancer Ther 2004, 3, 149. [PubMed: 14985455]

[47]. Sokolova E, Kutova O, Grishina A, Pospelov A, Guryev E, Schulga A, Deyev S, Balalaeva I, Pharmaceutics 2019, 11, DOI 10.3390/pharmaceutics11050219.

[48]. Beyer I, Cao H, Persson J, Song H, Richter M, Feng Q, Yumul R, Van Rensburg R, Li Z, Berenson R, et al., Clin. Cancer Res 2012, 18, 3340. [PubMed: 22535153]

[49]. Tannock IF, Lee CM, Tunggal JK, Cowan DSM, Egorin MJ, Clin. Cancer Res 2002, 8, 878. [PubMed: 11895922]

[50]. Fayad W, Brnjic S, Berglind D, Blixt S, Shoshan MC, Berndtsson M, Olofsson MH, Linder S, Int. J. Cancer 2009, 125, 2450. [PubMed: 19670329]

[51]. Kim H, Mun S, Choi Y, J. Mater. Chem. B 2013, 1, 429. [PubMed: 32260811]

[52]. Burleson KM, Boente MP, Pambuccian SE, Skubitz APN, J. Transl. Med 2006, 4, 1. [PubMed: 16390546]

[53]. Fischer ER, Hansen BT, Nair V, Hoyt FH, Dorward DW, Curr Protoc Microbiol 2012, 25, 2B.2.1.

[54]. Lee HR, Pelaez F, Silbaugh AM, Leslie F, Racila E, Azarin SM, ACS Appl. Bio Mater 2019, 2, 1549.

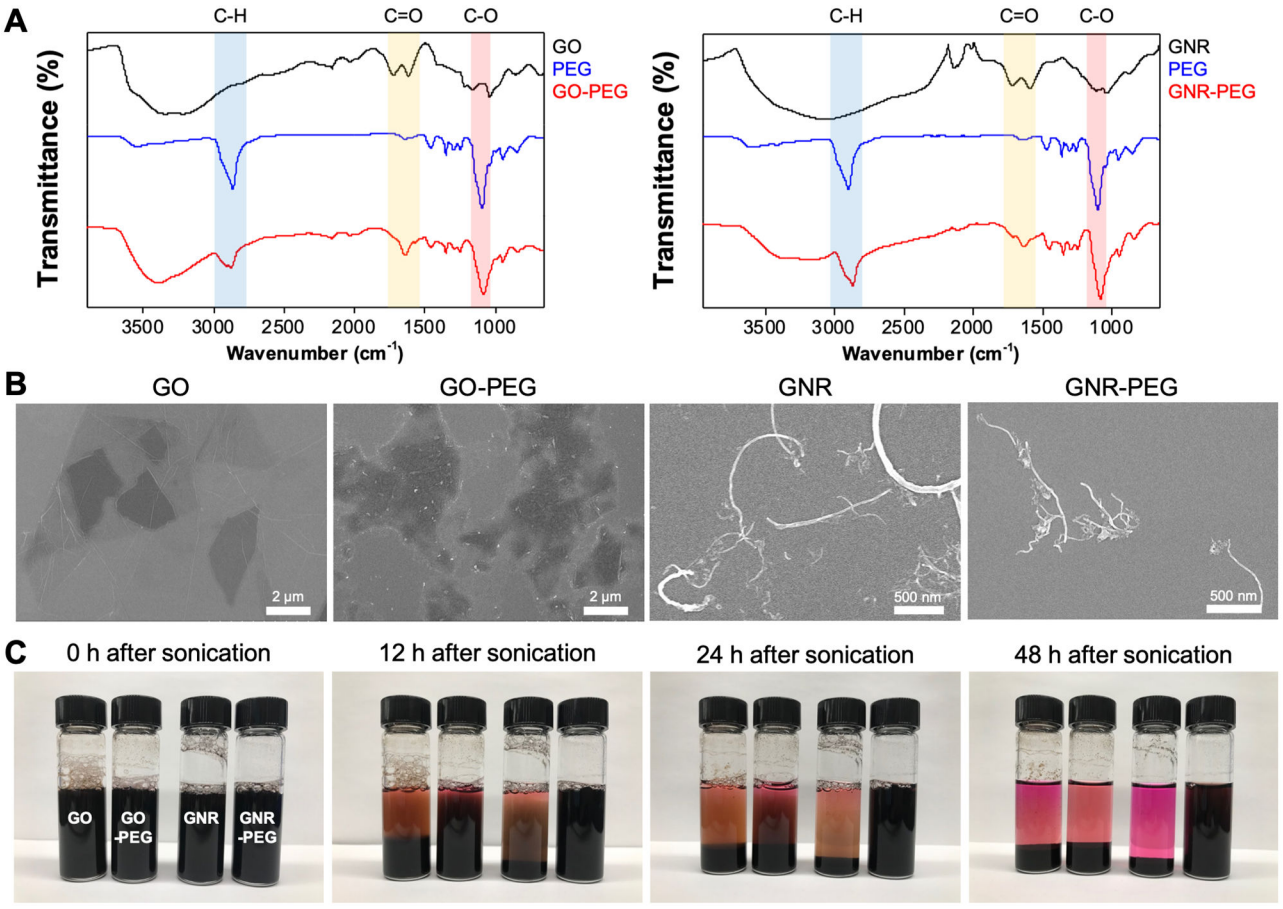

Figure 1.

PEGylation of GO and GNR to reduce aggregation in protein-rich ascites. (A) FTIR spectra of GO-PEG (left) and GNR-PEG (right). Signature peaks of 4-arm PEG were detected in the FTIR spectra of GO-PEG and GNR-PEG: C-O stretch (red region at ~1100 cm^{-1}), COO-H/O-H stretch (blue region at ~2850 cm^{-1}), and C=O stretch (yellow region at ~1640 cm^{-1}). (B) Representative SEM images of GO, GO-PEG, GNR, and GNR-PEG revealed no significant morphological changes after PEGylation. (C) Aggregation test in cell culture media containing 20% (v/v) serum (FBS). Graphene-based materials (100 μg mL^{-1}) settled over time in serum-rich media due to aggregation.

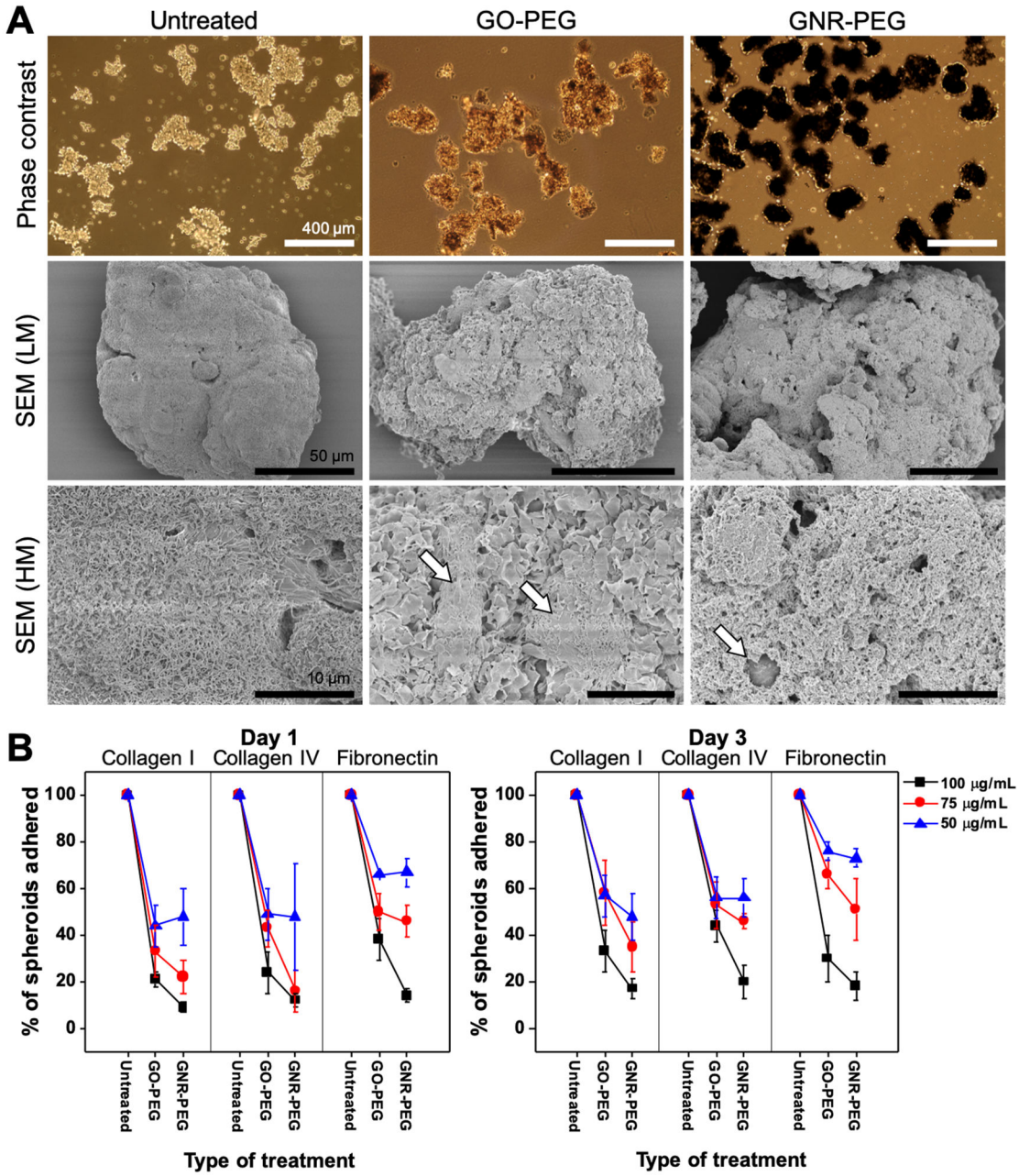

Figure 2.

GO-PEG and GNR-PEG disrupt adhesion of SKOV-3 spheroids to ECM proteins abundant in the mesothelial layer. (A) Representative phase contrast and SEM images of SKOV-3 spheroids (LM; low magnification, HM; high magnification). Scale bars indicate 400 μm in phase contrast images and 50 μm (LM) or 10 μm (HM) in SEM images. The white arrows in SEM (HM) images indicate exposed cell surfaces. (B) Percentage of total spheroids that have adhered after 1 or 3 days of incubation on collagen I, collagen IV, or fibronectin.

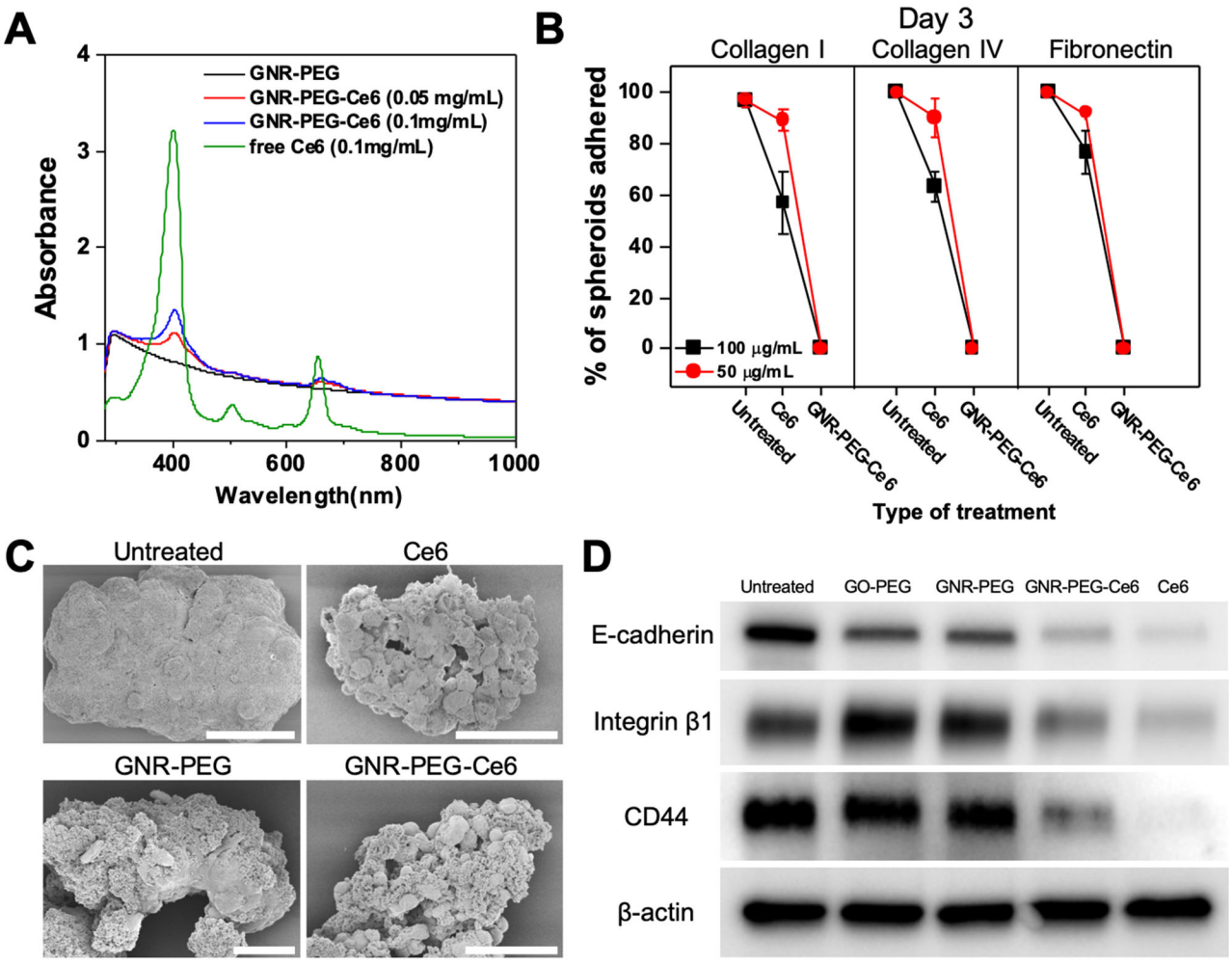

Figure 3.

Ce6 loading onto GNR-PEG further reduces spheroid adhesion to ECM proteins by downregulating surface receptor proteins. (A) UV-VIS spectra of free Ce6, GNR-PEG, and GNR-PEG-Ce6. (B) Percentage of total spheroids that have adhered after 3 days of incubation on collagen I, collagen IV or fibronectin. (C) Representative SEM images of untreated, Ce6-treated, GNR-PEG-treated, and GNR-PEG-Ce6-treated SKOV-3 spheroids. Scale bars indicate 50 μm. (D) Western blot analysis of protein expression in untreated, GO-PEG-treated, GNR-PEG-treated, GNR-PEG-Ce6-treated, and Ce6-treated SKOV-3 spheroids after 48 h of treatment.

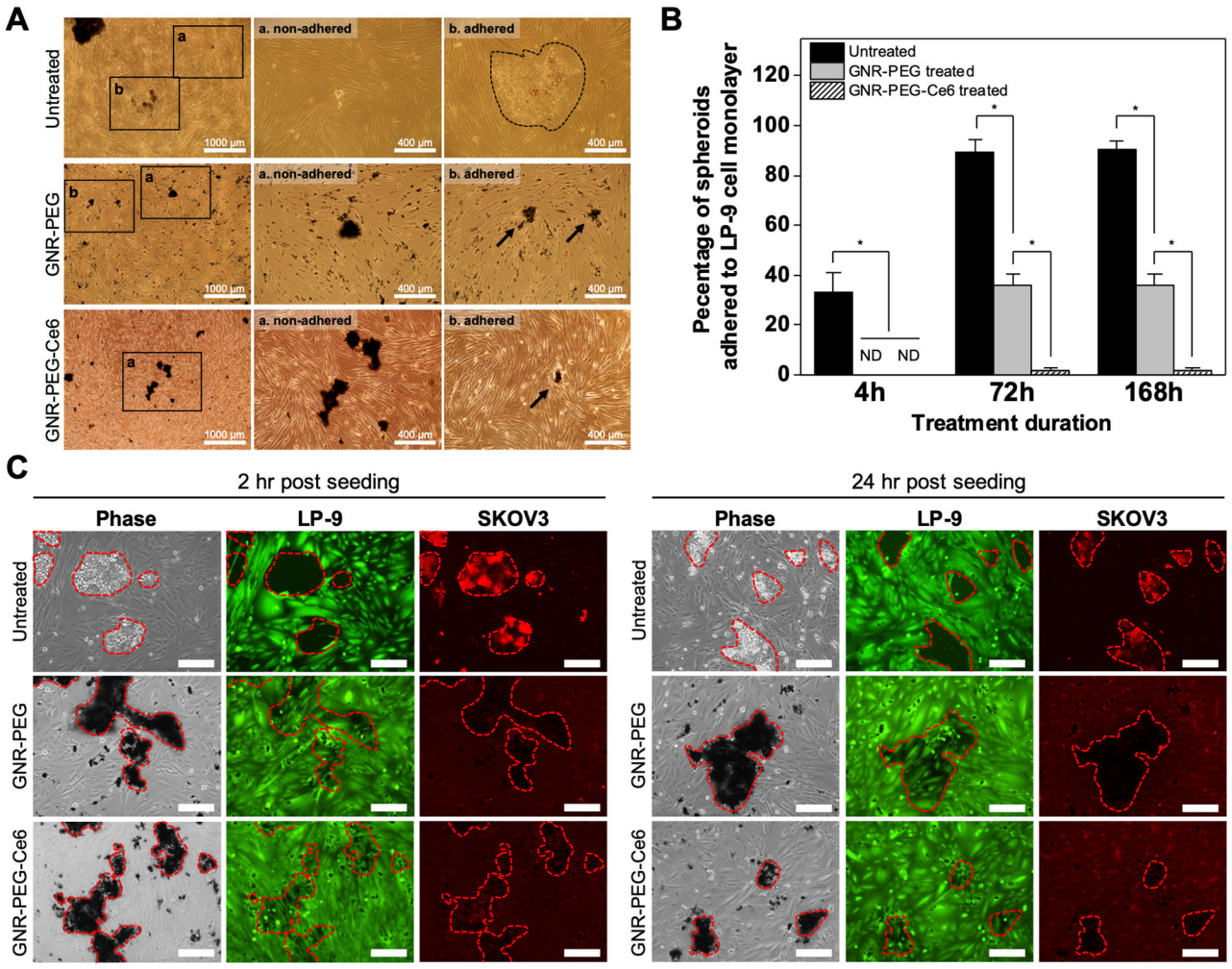

Figure 4.

GNR-PEG-Ce6 disrupts mesothelial adhesion of SKOV-3 spheroids and subsequent mesothelial clearance. (A) Representative phase contrast images of adhered and non-adhered spheroids in each condition after 72 h of incubation. (B) Percentage of total spheroids that have adhered to the LP-9 mesothelial cell layer after 4, 72, or 168 h of incubation (*P < 0.05, ND indicates not detected). (C) Representative phase contrast images of SKOV-3 spheroids breaching the underlying LP-9 monolayer and corresponding fluorescence images of the LP-9 monolayer (green) and SKOV-3 spheroids (red) at 2 or 24 h after spheroid seeding. Scale bars indicate 200 μm.

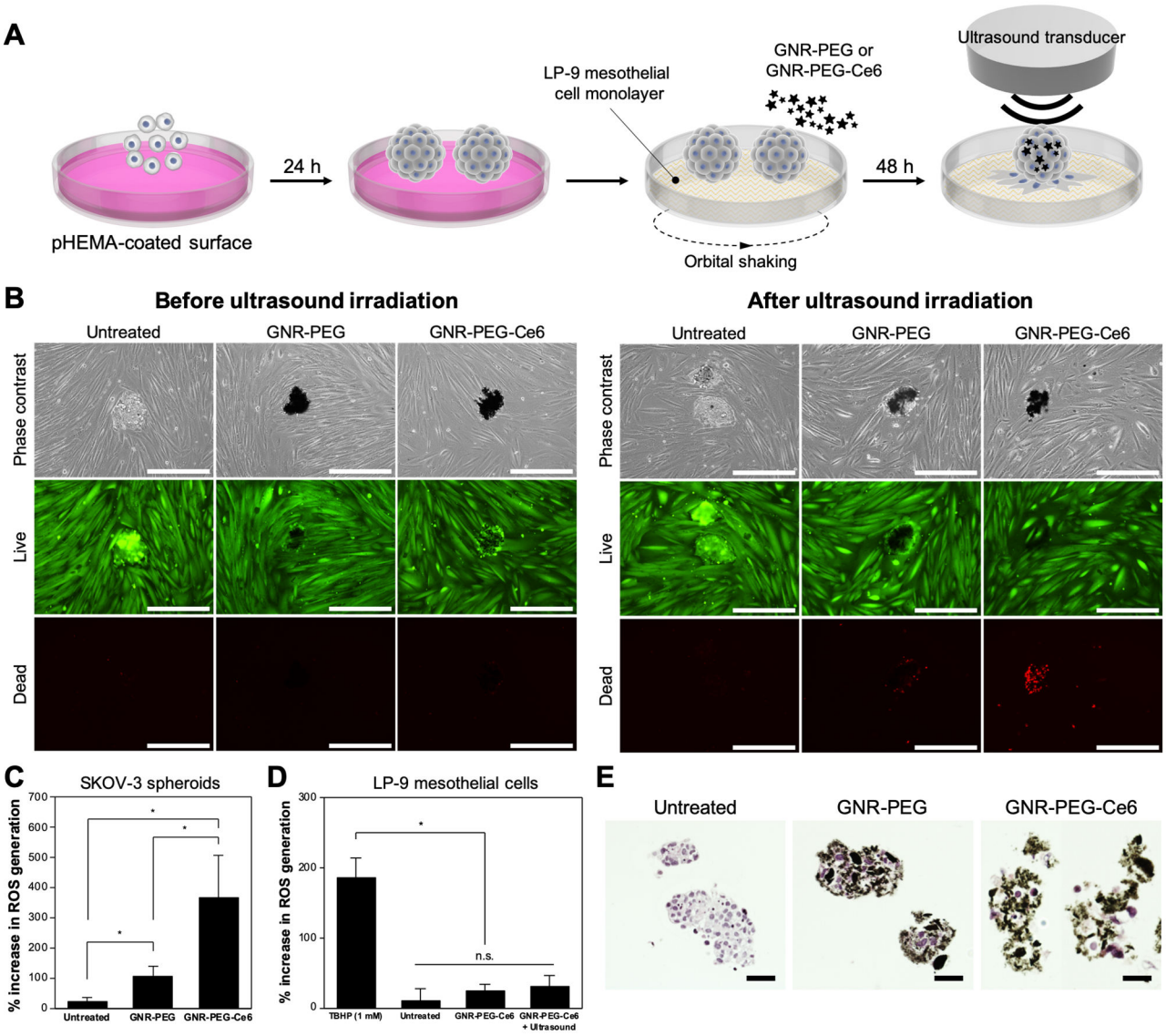

Figure 5.

GNR-PEG-Ce6 can kill adhered ovarian cancer spheroids via sonodynamic therapy. (A) Schematic of the process for ultrasound irradiation of adhered spheroids. (B) Representative images of live (green) and dead (red) cells in untreated, GNR-PEG-treated, and GNR-PEG-Ce6-treated SKOV-3 spheroids adhered to the LP-9 mesothelial cell layer before and after ultrasound irradiation. Scale bars indicate 400 μm. (C, D) ROS generation in SKOV-3 spheroids (C) and LP-9 mesothelial cells (D) after ultrasound irradiation (*$P < 0.05$). Tert-butyl hydrogen peroxide (TBHP) was used as a positive control in this assay. (E) Hematoxylin and eosin-stained (histological) cross-sections of untreated, GNR-PEG-treated, and GNR-PEG-Ce6-treated SKOV-3 spheroids. Scale bars indicate 50 μm.

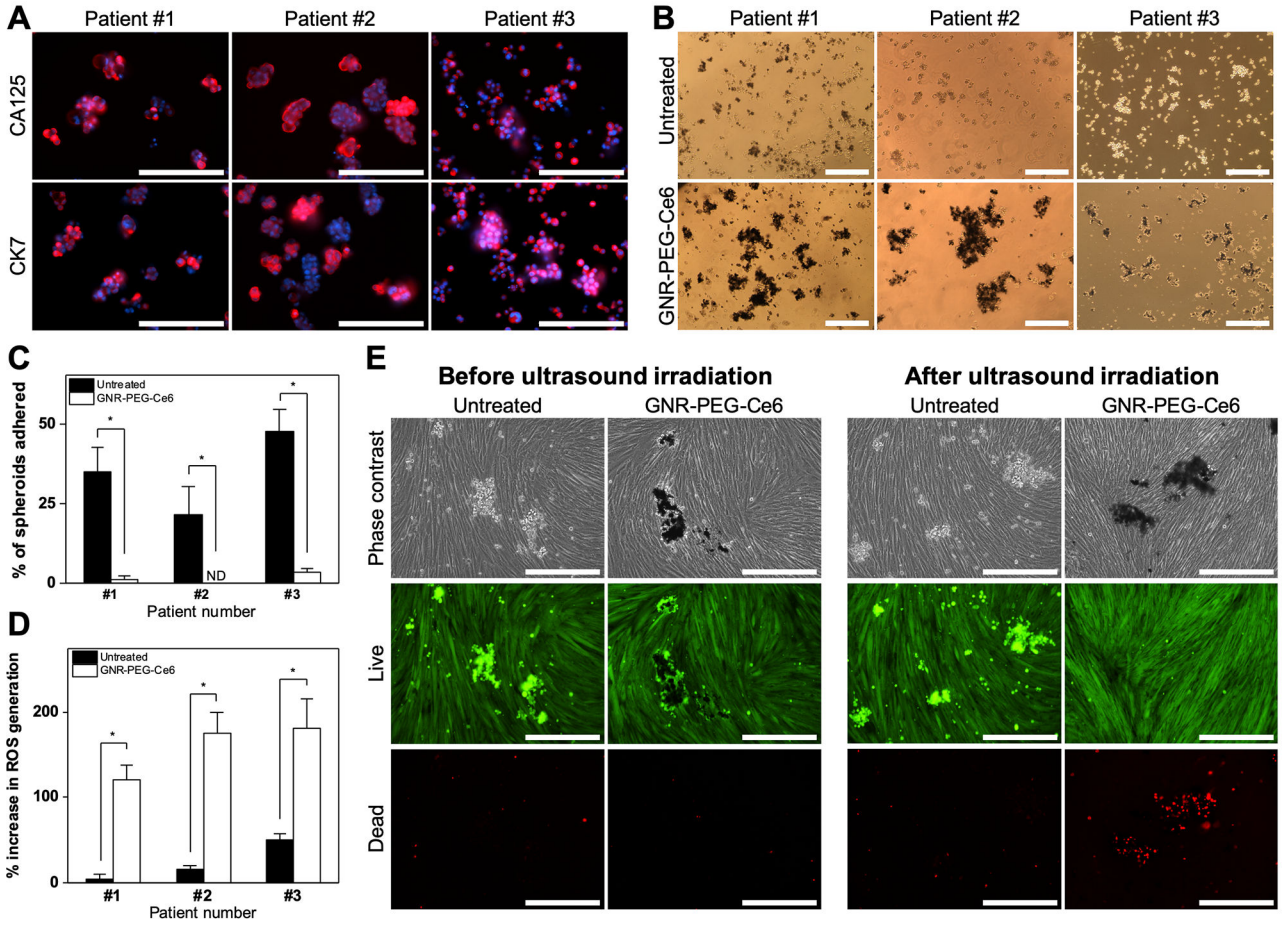

Figure 6.

GNR-PEG-Ce6 can disrupt mesothelial adhesion of patient ascites spheroids and destroy them via sonodynamic therapy. (A) Representative immunofluorescence images of CA125 and CK7 expression in patient ascites spheroids. Scale bars indicate 200 μm. (B) Representative phase contrast images of untreated and GNR-PEG-Ce6-treated patient ascites spheroids. Scale bars indicate 400 μm. (C) Percentage of total patient ascites spheroids that have adhered to the LP-9 mesothelial cell layer after 72 h of incubation (*$P < 0.05$; ND indicates not detected). (D) ROS generation in patient ascites spheroids after 30 s of 0.8 W cm^{-2} ultrasound irradiation (*$P < 0.05$). (E) Representative images of live (green) and dead (red) cells in untreated and GNR-PEG-Ce6 treated patient ascites spheroids that have adhered to the LP-9 mesothelial cell layer before and after ultrasound irradiation. Scale bars indicate 400 μm.